**SANDIA REPORT**
SAND2022-11604
Printed August 2022

Sandia National Laboratories

# Improving Common PV Module Temperature Models by Incorporating Radiative Losses to the Sky

Anton Driesse, Joshua S. Stein, Marios Theristis

Prepared by
Sandia National Laboratories
Albuquerque, New Mexico
87185 and Livermore,
California 94550

Issued by Sandia National Laboratories, operated for the United States Department of Energy by National Technology & Engineering Solutions of Sandia, LLC.



Available to DOE and DOE contractors from
U.S. Department of Energy
Office of Scientific and Technical Information
P.O. Box 62
Oak Ridge, TN 37831

Telephone: (865) 576-8401
Facsimile: (865) 576-5728
E-Mail: reports@osti.gov
Online ordering: http://www.osti.gov/scitech

Available to the public from
U.S. Department of Commerce
National Technical Information Service
5301 Shawnee Rd
Alexandria, VA 22312

Telephone: (800) 553-6847
Facsimile: (703) 605-6900
E-Mail: orders@ntis.gov
Online order: https://classic.ntis.gov/help/order-methods/

## ABSTRACT

PV module operating temperature is the second-most important factor influencing PV system yield—after irradiance—and a substantial contributor to uncertainty in energy system yield predictions. Models commonly used to predict operating temperature in system simulations are based on a simplified energy balance that lumps together different heat loss mechanisms—including radiation—and assumes an overall linear behavior. Radiative heat loss to the sky is usually substantial, but modeling it accurately requires additional information about down-welling long-wave radiation or sky temperature and increases the complexity of temperature model equations.

In this work we show how radiative losses to the sky can be separated into two parts to improve the accuracy of modeling without additional complexity. We also predict and demonstrate the variation of these losses at different tilt angles and show that the effective view factor is reduced by the non-isotropic distribution of down-welling long-wave radiation. Finally, we demonstrate substantial reduction in bias (MBE) and scatter (RMSE) when the new radiative loss term is added to the Faiman model using one year of measurements at Sandia National Labs.

## CONTENTS



## LIST OF FIGURES

## LIST OF TABLES

## ACRONYMS AND TERMS

| Acronym/Term | Definition |
|---|---|
| ε | emissivity (in particular in the infrared region) |
| F | view factor (in particular view factor from a PV module to the sky) |
| NOCT | nominal operating cell temperature |
| PV | photovoltaic |
| SAPM | Sandia array performance model |
| $T_a$ | ambient temperature |
| $T_m$ | module temperature |
| $T_s$ | equivalent sky temperature |
| U | heat loss coefficient |
| WS | wind speed |

## 1.0 INTRODUCTION

PV modules convert part of the absorbed solar radiation to thermal energy or heat, and as a result module temperature rises. As the temperature rises, the rate of heat loss to the environment increases until the loss rate matches the gain rate from solar energy absorption. At that equilibrium point the temperature would remain stable if all other conditions remain constant; however, air temperature, wind speed and other external conditions vary continuously such that module temperature is rarely stable. Module temperature is the second-most important factor influencing PV system yield, but since simulations of PV systems have historically used (and still usually use) one-hour time-steps, the dynamics of temperature fluctuations are usually ignored. Instead, so-called steady-state thermal models are used which assume the average conditions over the hour are constant.

The steady-state thermal models most commonly used in simulation software for yield assessment and energy rating are one-dimensional, linear, lumped-parameter models with empirically determined coefficients: Faiman [1], SAPM [2], PVsyst [3], SAM-NOCT [4]. This means they use just a few parameters to represent all the complexities of the heat exchange between the module and its environment, and indeed also of the heat generation and transfer within the module. Heat flow is assumed to occur only in the direction perpendicular to the PV module surface, which makes them one-dimensional models. The rate of heat rejection varies linearly with the difference between module temperature ($T_m$) and ambient temperature ($T_a$), which means that when $T_m$ equals $T_a$, no heat can be rejected according to the models. In reality, however, a substantial amount of heat is usually rejected under this condition because of the long-wave radiation exchange with the colder sky. This is very much apparent at night when module temperatures frequently drop below ambient temperature, but this exchange also takes place during the day.

The Fuentes model [5] implemented in PVWATTS v5 (and earlier versions) is an exception to the above description as it incorporates the estimation of sky temperature and radiative losses to the sky. Consequently the model predicts module temperatures several degrees below ambient in the first and last hours of each day when irradiance is low. However, the model incorporates several default behaviors and unfamiliar parameters, and it has not been adopted by any other mainstream software. In fact, the latest version of PVWATTS v8 no longer uses the Fuentes temperature model but has been changed to the SAM-NOCT model in order to be more consistent with the SAM software [6].

In this work a practical method is presented for incorporating radiative losses to the sky dome into any of the existing one-dimensional linear lumped-parameter models. Since radiative losses are site-dependent this offers a two-fold advantage: the parameters for the modified models become less site-dependent, and at the same time operating temperature predictions using the modified models become more site-specific. These advantages could be desirable in a range of applications from energy rating to yield assessments and from performance metrics to digital twinning.

## 2.0 BACKGROUND: THERMAL BALANCES EVERYWHERE

Although "thermal balance" or "heat transfer" labels are often used to tag more advanced modeling efforts that go back to first principles, all the simple lumped parameter models in use actually describe a thermal balance between a PV module and its environment—it's just a less detailed and exact balance. A high-level, steady-state, thermal balance (disregarding thermal capacitance) is expressed by the following equation:

$$q_{sun} - q_{elec} - q_{rad} - q_{conv} - q_{cond} = 0 \quad (1)$$

where $q_{sun}$ is the energy flux from the sun, $q_{elec}$ the energy flux extracted as electrical power, and the remaining three terms are the heat losses by radiation, convection and conduction (all in W/m$^2$). Conduction is usually negligible since the area of contact between the PV module frame and mounting structure is very small, and it will therefore not be mentioned further.

Figure 1 illustrates how an energy balance might evolve during a sunny day in Albuquerque, and the temperatures corresponding to this energy balance are shown in Figure 2. For the purpose of the illustration the individual energy fluxes are approximated as follows:

- *Solar* is the measured plane-of-array irradiance.
- *Electrical* is 16% of *Solar* (constant efficiency).
- *Radiative* loss to the sky and ground are calculated from measured module temperature and estimated sky and ground temperatures respectively using an emissivity of 0.88 and view factor of 1.0. Sky temperature is calculated from pyrgeometer readings and ground temperature is assumed to be equal to air temperature.
- *Conduction* through the module frame is assumed to be zero.
- *Convection* is the amount needed to balance the other flows.

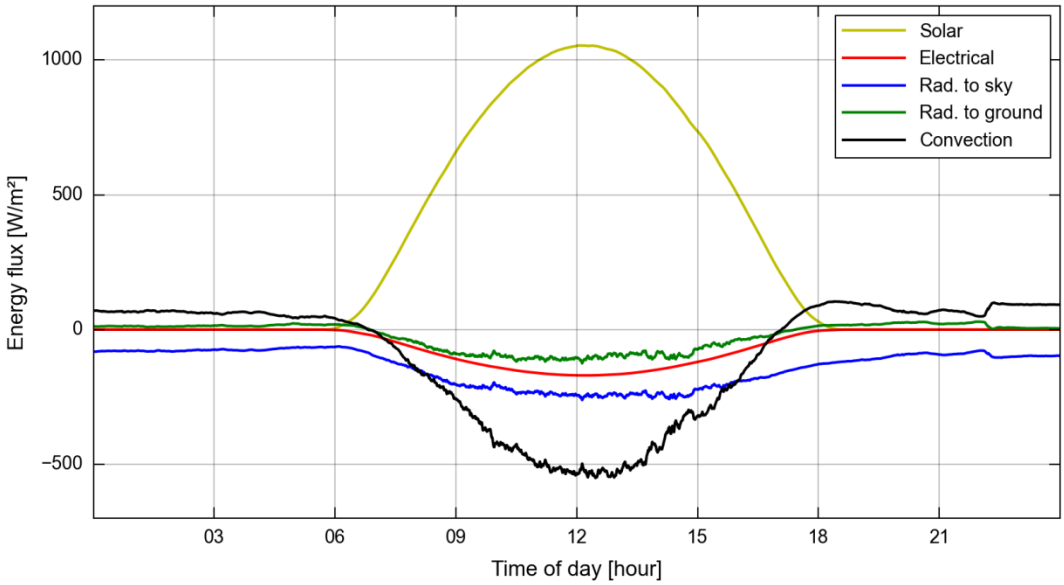


**Figure 1 Energy flows into and out of a PV module over the course of a sunny day (Sept. 9, 2016) in Albuquerque, NM.**

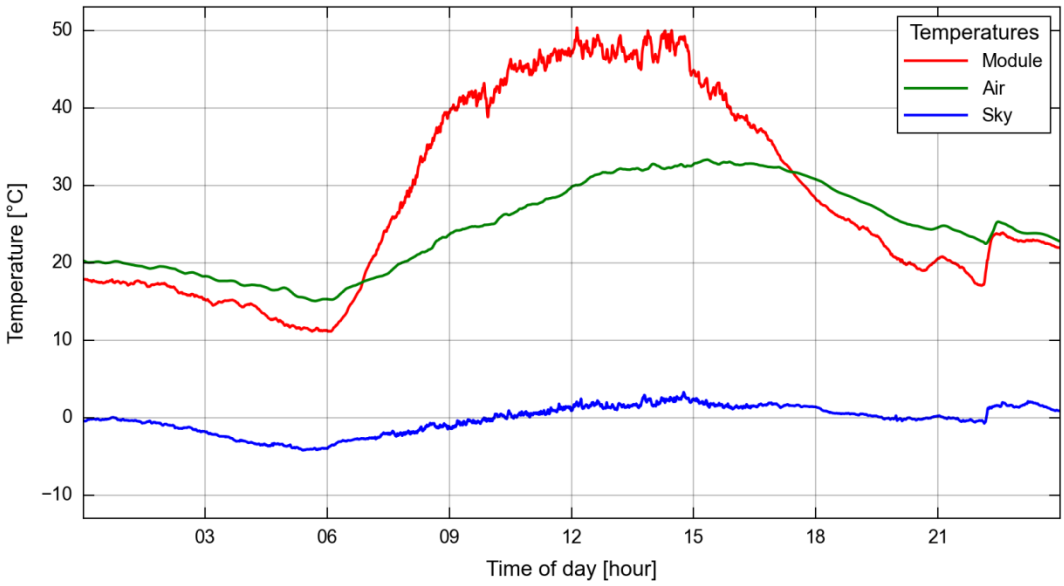


**Figure 2 Estimated sky and measured air and module temperatures over the course of a sunny day (Sept. 9, 2016) in Albuquerque, NM. Effective sky temperature is calculated from pyrgeometer measurements of long-wave radiation.**

The most prominent feature of Figure 2 is the substantial and rapid fluctuation in module temperature, which is caused by fluctuations in wind speed that alter the rate of convective cooling. However, the most *important* feature for this report is the fact that module temperature descends well below ambient air temperature at night. This is due to radiative losses to the sky, which has an effective temperature that is much lower than the ambient temperature. As Figure 1 shows, the night-time radiative losses are balanced by energy gains through convection; i.e., the surrounding air provides the energy that is radiated out. This is not only a night-time phenomenon but heat is lost to the sky by radiation throughout the day, and must therefore be included in some way in PV module temperature models.

The simplest way to include radiative losses is to lump them together with the convective losses:

$$q_{sun} - q_{elec} - q_{cr} = 0 \tag{2}$$

Although $q_{cr}$ actually depends on a large number of parameters and properties, its main tendency is to increase as the temperature of the module ($T_m$) rises above the temperature of the environment ($T_a$). Using a one-dimensional, linear approximation of this tendency produces the thermal balance equation:

$$q_{sun} - q_{elec} - U_{cr} \cdot (T_m - T_a) = 0 \tag{3}$$

where $U_{cr}$ is the combined or lumped heat loss coefficient representing transfer by both convection and radiation. This can easily be rearranged to calculate module temperature:

$$T_m = T_a + \frac{q_{sun} - q_{elec}}{U_{cr}} \tag{4}$$

However, $q_{sun}$ is always positive and $q_{elec}$ must be smaller than $q_{sun}$; therefore, this equation cannot model module temperatures that fluctuate both above and below ambient temperatures as they do in reality.

The electrical power output can be handled in two different ways. It can be left where it is in (4), but since $q_{elec}$ is approximately proportional to $q_{sun}$ (i.e. $q_{elec} = q_{sun} \times module\ efficiency$) it is also possible to incorporate it into the heat loss coefficient by scaling the latter:

$$T_m = T_a + \frac{q_{sun} \cdot (1 - module\ efficiency)}{U_{cr}}$$

$$T_m = T_a + \frac{q_{sun}}{\left[\frac{U_{cr}}{1 - module\ efficiency}\right]}$$

$$T_m = T_a + \frac{q_{sun}}{U} \tag{5}$$

We will move forward with this simplified linear equation. A second linear approximation usually finds its way into this equation to represent the fact that wind enhances cooling, and therefore increases the value of the combined heat transfer coefficient $U$. This leads to an equation for module temperature that most closely resembles the Faiman model, but is also fundamentally equivalent to the PVsyst and SAM NOCT models:

$$T_m = T_a + \frac{q_{sun}}{u_0 + u_1 \cdot WS} \tag{6}$$

In the Faiman model $q_{sun}$ is equated with plane-of-array irradiance ($G_{poa}$), whereas in the PVsyst and SAM NOCT models the value of $G_{poa}$ is reduced to account for the facts that some of the incidence energy is reflected, and some is extracted as electricity. Although it looks different at first sight, the SAPM model also fits this template. It differs only in the formulation of $U$, which has a non-linear wind coefficient:

$$U = e^{-(a+b \cdot WS)} \tag{7}$$

These four models require different values for their model coefficients but have very similar overall behavior. In fact, their equivalence has been analyzed in detail in [7] and functions that translate the coefficients between models are available in pvlib-python [8] It is important to establish this equivalence between the models and view them all as thermal balance calculations because this is the reason why the proposed adjustment for radiative losses can be used to improve any or all of them.

# 3.0 MODEL DEVELOPMENT

## 3.1 The radiative loss term

In this section we examine the exact calculations for radiative losses and propose a simplification that is more realistic than the lumped heat transfer coefficient, yet still easy to use. An intuitive way to formulate the radiative exchange between the module and sky is by using an effective sky temperature, $T_s$:

$$q_{rad} = F \cdot \varepsilon \cdot \sigma \cdot (T_m^4 - T_s^4) \tag{8}$$

where $F$ is the view factor or configuration factor between the module and the sky, $\varepsilon$ is the emissivity of the module surface facing the sky, and $\sigma$ is the Stefan-Boltzmann constant with a value of $5.7 \times 10^{-8}$ W/m$^2$/K$^4$. $T_s$ cannot be measured directly but is an abstract value that represents the downward radiation from the atmosphere to the module. When Eq.(8) is inserted into the thermal balance, the resulting equation can no longer be rearranged into closed form to find $T_m$ but must be solved by numerical methods instead, for example fixed-point iteration. This is not a major challenge for a computer programmer and certainly less complex than finding the maximum power point for the single-diode PV cell model, but traditionally linear simplifications tend to be preferred as they permit even complex thermal systems to be analyzed and solved more easily.

The usual way to simplify the radiative exchange is to assume linear behavior over the range of temperatures of interest; however, this blurs the distinction between radiative and convective losses and leads to the use of a single lumped heat transfer coefficient. What we propose instead, is to split the radiative loss to the sky into two parts, $q_{rad,m}$ and $q_{rad,s}$, using the ambient temperature, $T_a$, as a common reference temperature:

$$q_{rad,m} = F \cdot \varepsilon \cdot \sigma \cdot \left(T_m^4 - T_a^4\right) \tag{9}$$

$$q_{rad,s} = F \cdot \varepsilon \cdot \sigma \cdot (T_a^4 - T_s^4) \tag{10}$$

$$q_{rad} = q_{rad,m} + q_{rad,s} \tag{11}$$

$q_{rad,s}$ does not depend on $T_m$ and can therefore be evaluated without simplification in a module temperature calculation (provided $T_a$ and $T_s$ are known). Only $q_{rad,m}$ is linearized in the usual way:

$$q_{rad,m} = u_{rad,m} \cdot (T_m - T_a) \tag{12}$$

creating a heat transfer coefficient $u_{rad,m}$ and the thermal balance equation:

$$q_{sun} - F \cdot \varepsilon \cdot \sigma \cdot (T_a^4 - T_s^4) - (u_{rad,m} + u_{conv}) \cdot (T_m - T_a) = 0 \tag{13}$$

Finally, $u_{rad,m}$ is merged (lumped) with $u_{conv}$ and module temperature can be calculated explicitly as:

$$T_m = T_a + \frac{q_{sun} - F \cdot \varepsilon \cdot \sigma \cdot (T_a^4 - T_s^4)}{U} \tag{14}$$

This model relies on one additional input variable, $T_s$, and has two additional parameters, $F$ and $\varepsilon$, compared to Eq. (7). With these small changes the radiative losses to the sky can be introduced easily into the numerator of all four linear temperature models.

Nevertheless one small detail should be changed. Sky temperature is a convenient way to think about (and calculate) net radiative exchange with the atmosphere, but it is really an indirect way of representing down-welling thermal radiation. We prefer to make down-welling radiation $q_{dr}$ itself an input parameter for the model since this is the quantity available from databases and measurements. Therefore, the final model equation in generic form is:

$$T_m = T_a + \frac{q_{sun} - F \cdot \varepsilon \cdot \left(\sigma \cdot T_a^4 - q_{dr}\right)}{U} \tag{15}$$

Using the Faiman / IEC 61853 nomenclature this becomes:

$$T_m = T_a + \frac{G_{poa} - F \cdot \varepsilon \cdot \left(\sigma \cdot T_a^4 - q_{dr}\right)}{u_0 + u_1 \cdot WS} \tag{16}$$

The PVsyst variant can also be improved as follows:

$$T_m = T_a + \frac{G_{poa} \cdot \alpha \cdot (1 - \eta) - F \cdot \varepsilon \cdot \left(\sigma \cdot T_a^4 - q_{dr}\right)}{u_c + u_v \cdot WS} \tag{17}$$

Similarly for the SAM NOCT variant:

$$T_m = T_a + \frac{G_{poa} \cdot \tau\alpha - G_{poa} \cdot \eta - F \cdot \varepsilon \cdot \left(\sigma \cdot T_a^4 - q_{dr}\right)}{U_L} \tag{18}$$

And finally the SAPM model:

$$T_m = T_a + \frac{G_{poa} - F \cdot \varepsilon \cdot \left(\sigma \cdot T_a^4 - q_{dr}\right)}{e^{-(a+b \cdot WS)}} \tag{19}$$

To use any of these improved models for a PV system simulation we simply need down-welling radiation data, values for the new parameters $F$ and $\varepsilon$ as well as the modified values for the original heat-transfer coefficients. These are discussed in the following two sections.

## 3.2 Model input: downward radiation

There are at least three ways to obtain downward radiation data: from pyrgeometer measurements, from published correlations with other weather parameters, and from global weather models. Pyrgeometer measurements are rarely collected at photovoltaic plants or testing facilities, therefore a model requiring them might not find broad acceptance. An established alternative to direct measurement is to use one of many correlations with air temperature, humidity, time of day, and/or other commonly available parameters to estimate sky temperature (and indirectly the down-welling radiation). One caveat with this option is that many of these correlations are specifically for cloud-free conditions; this is the reason why the Fuentes model [5], which has such a correlation built-in, predicts below ambient module temperatures even under cloudy skies.

Historically, correlations were the only alternative to on-site measurements, but in recent years easier access to global weather and climate model data has created another viable option. Global weather models must take into account short and long-wave radiation exchanges between the earth and sky, and even between different layers of the atmosphere in order to calculate energy flows and balances. Thus down-welling radiation at the earth's surface is one of the many parameters they produce as a byproduct. The main drawbacks of this source compared to local pyrgeometer measurements are the

coarse spatial and temporal resolution. However, the data are relatively easy to obtain and have global coverage; therefore, lack of suitable data cannot be considered an obstacle to integrating radiative thermal losses into standard practice for PV system simulations. ERA5 is one such global dataset; documentation and download instructions for ERA5 are found in [9].

## 3.3 Model parameters: view factor and emissivity

The view factor and emissivity are present in the model only as a product, $(F \cdot \varepsilon)$ which means that they could be replaced by a single parameter. However, it is important that they be kept distinct because the view factor is a function of tilt angle, which is an aspect of the installation, whereas emissivity is a property of the PV module.

PV modules emit thermal radiation in all directions. However, the areas of the edges are very small therefore it should be sufficient to consider only the front and back surfaces. These may consist of different materials having different emissivities: values in the range 0.84 to 0.91 are reported for glass surfaces whereas polymer backsheets range from 0.85 to 0.89 [10]–[12]. The precise type of glass or back sheet is rarely identified in the scientific literature or on PV module spec sheets, which adds further uncertainty to the thermal modeling.

The other unknown parameter is the view factor F. It is tempting to apply the same view factor calculations for thermal radiation that are used for short-wave diffuse sky irradiance, but this would be incorrect since the anisotropy is very different. Positive downward radiation is much lower near the zenith and increases near the horizon, thus the net radiative loss to the zenith region is much higher than to the horizon region. This can be clearly seen in the sample thermal sky images in Figure 3. The precise distribution varies over time and depends on cloud cover and atmospheric conditions, so the use of a single constant view factor is an oversimplification of reality. Nevertheless, it is possible to make a few approximations to obtain the range of values that can be expected. At one extreme lies the isotropic hemispherical sky and at the other extreme the sky is represented by a single point at the zenith. As Table 1 shows, for moderate tilt angles the view factors for these two extreme cases do not lie very far apart, therefore their average value could be considered a reasonable first estimate for the long-wave radiation view factor.

Note that these estimates are only for the front surface. With moderate tilt angles the back of the module will primarily see the ground and warmer horizon area of the sky, therefore net radiative losses from the rear of the module to the sky should be much smaller.

**Table 1 Expected values of the $F \cdot \varepsilon$ product**

| Tilt angle | Isotropic assumption | Zenith-only assumption | Average F | $F \cdot \varepsilon$ | Change from horizontal |
|---|---|---|---|---|---|
| β | F1 = (1 + cos β) / 2 | F2 = cos β | F = (F1 + F2) / 2 | ε=0.88 | |
| 0° | 1.00 | 1.00 | 1.000 | 0.88 | |
| 25° | 0.95 | 0.91 | 0.930 | 0.82 | -7% |
| 35° | 0.91 | 0.82 | 0.865 | 0.76 | -14% |
| 37.5° | 0.90 | 0.79 | 0.845 | 0.74 | -16% |

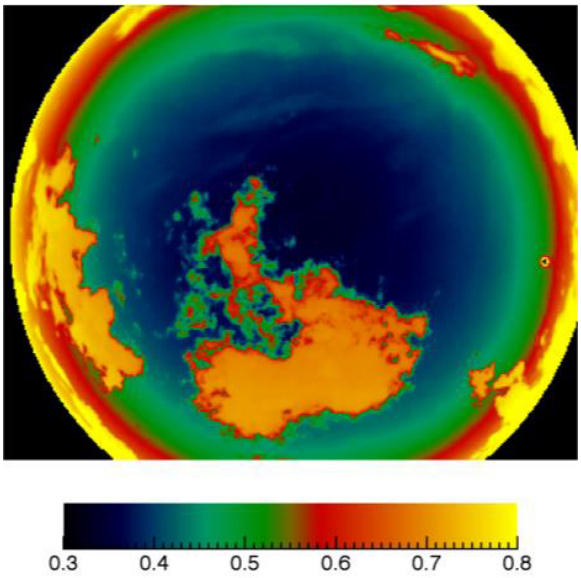


**Figure 3 Relative magnitude of infrared downward radiation recorded by a sky camera system, showing the strong contrast between the cold zenith region (cloud-free), a warmer cloudy area near the zenith and the warm horizon. [13]**

# 4.0 EXPERIMENTAL VALIDATION

## 4.1 Method

Using the models discussed thus far, it is not possible to obtain separate values for emissivity and view factor by fitting the models to field data; however, it is possible to obtain their product. This is not trivial because $F{\cdot}\varepsilon$ is quite strongly correlated with the existing combined heat transfer coefficients. Furthermore, these models only represent steady-state conditions whereas measurements of module temperature are naturally somewhat delayed with respect to changes in irradiance and wind speed. The way to circumvent both of these problems is to select only measured data points where the module temperature is very near to the ambient temperature, e.g. within ±0.5 °C or less, where the loss by convection is very small. These conditions usually occur very early or late in the day when irradiance is mostly diffuse, so near steady-state conditions can also be expected.

In the absence of convective losses the incoming short-wave irradiance should balance the radiative thermal loss to the sky simplifying the thermal balance to:

$$q_{sun} - F \cdot \varepsilon \cdot \left(\sigma \cdot T_a^4 - q_{dr}\right) = 0 \tag{20}$$

The product $F{\cdot}\varepsilon$ can then in principle be calculated as the mean ratio of incoming short-wave radiation and net outgoing long-wave radiation:

$$F \cdot \varepsilon = \frac{q_{sun}}{\sigma \cdot T_a^4 - q_{dr}} \tag{21}$$

In practice, using Eq.(21) produced inconsistent results because the selected points may be non-uniformly distributed within the small temperature range. In fact, there are conflicting goals of narrowing the temperature range to minimize convection effects, and widening the temperature range to increase the number of points and obtaining a more representative average value. Therefore, the selected points were fitted to the more general energy balance of Eq. (13). This produces values for the convection parameters $u_0$, $u_1$ as well as $F{\cdot}\varepsilon$ but only the latter is retained. (Normally $u_0$ and $u_1$ would be recalculated in a second regression using a much larger selection of data points, but that is outside the scope of the present document.)

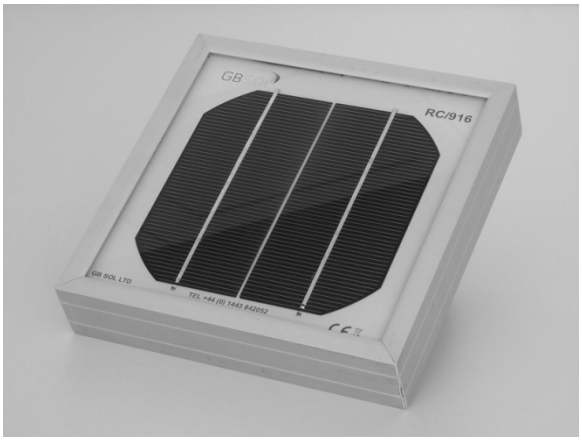


**Figure 4 Photograph of the reference cell type on which the measurements were taken, showing the module-like construction.**

## 4.2 Data sources and fitting procedure

We have chosen to demonstrate the determination of $F{\cdot}\varepsilon$ using data collected during the PVSENSOR project [14]. The test object is a reference cell that is constructed using the same materials and structure as a PV module (Figure 4). The dataset offers a number of useful features for this purpose:

- Irradiance is measured by the test object itself.
- Ambient and device temperatures are measured accurately by identical sensors and in close proximity to each other.
- Data are available at high temporal resolution (1s for irradiance and 10s for temperatures).
- Operation in two locations/climates can be compared: Albuquerque, NM and Freiburg, Germany.
- Physical mounting methods, temperature sensor and data acquisition details are largely identical between the two locations.
- Extensive reference instrumentation is located nearby, including pyrgeometers.
- Operation at different tilt angles (0 and 35) can be compared in Albuquerque.

As already mentioned, not all data points are used to determine $F{\cdot}\varepsilon$ but only those where module temperature is very near ambient temperature. The full selection criteria used for the results in this report are as follows:

- Difference between module and ambient temperature < 0.5 °C
- Wind speed < 3 m/s
- Solar zenith angle < 90° (sun above horizon)

Although the selected operating conditions tend to be fairly stable, 15-minute average values are nevertheless calculated to reduce noise.

The final selection criterion for the data is the time period of the measurements. The period of horizontal operation in Albuquerque is limited to the second half of September so this is a given constraint. To increase the chances of making a fair comparison with tilted operation the period from mid-August to mid-September was chosen for this. For Freiburg the data from mid-August to the end of September were used.

The parameter optimization then proceeds as follows: The left-hand side to of the energy balance equation is evaluated for all the selected time steps using an initial guess for the three parameters ($u_0$, $u_1$, $F{\cdot}\varepsilon$). The calculated energy imbalance values represent the model errors. The three parameters are then adjusted iteratively to minimize the sum of the squares of the model errors. The influence of outliers in this process is attenuated by optimizing the Huber loss function, rather than squared error as used in ordinary least squares. This is a form of robust parameter fitting that retains much of the sensitivity of squared error while reducing susceptibility to extrema. [15]

## 4.3 Results

In this section we first show the fitting results for one case in detail (35° tilt in Albuquerque) and then how all three cases produce $F{\cdot}\varepsilon$ values in the expected range as per Table 1.

Figure 5 plots measured module temperature rise vs. measured irradiance for relatively low irradiance conditions. The effect of radiant loss to the sky is clearly seen in the many points that lie below the x-axis. The red points near the x-axis (within ±0.5°C) are those used to determine $F{\cdot}\varepsilon$. by fitting.

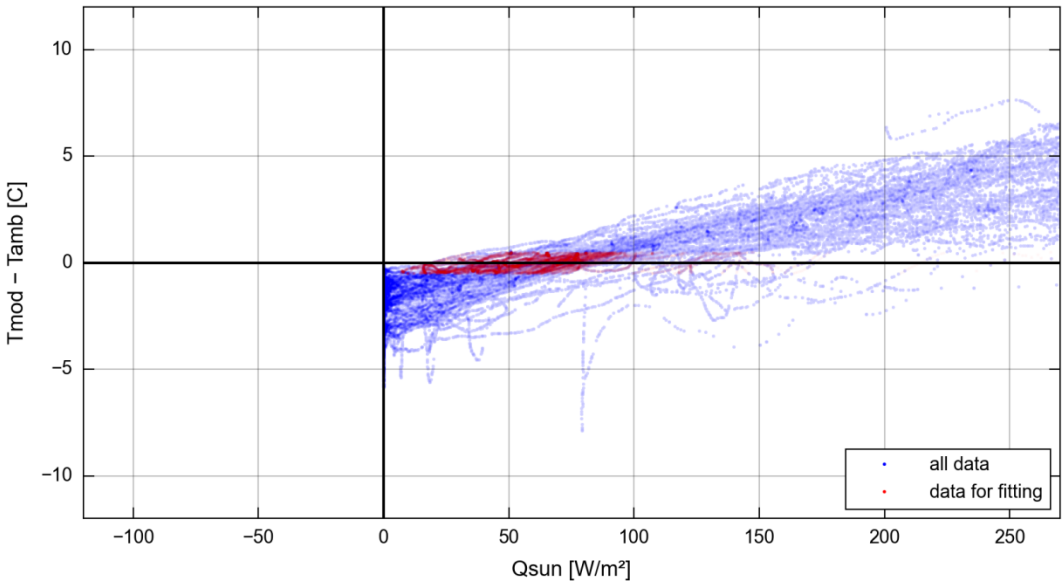


**Figure 5 Close-up of temperature rise vs. irradiance for the tilted reference cell in Albuquerque, showing cell temperatures below ambient even with positive irradiance. The red points are used to extract the value of *F·ε*.**

Figure 6 plots the same data set; however, the x-values are no longer solar irradiance but the net values obtained after subtracting the long-wave losses from the incoming short-wave radiation. The optimal $F \cdot \varepsilon$ value leads to the points used for fitting to lie clustered around the origin: here the temperature rise is near zero, therefore convection is near zero, and net radiation must also be near zero to complete the energy balance.

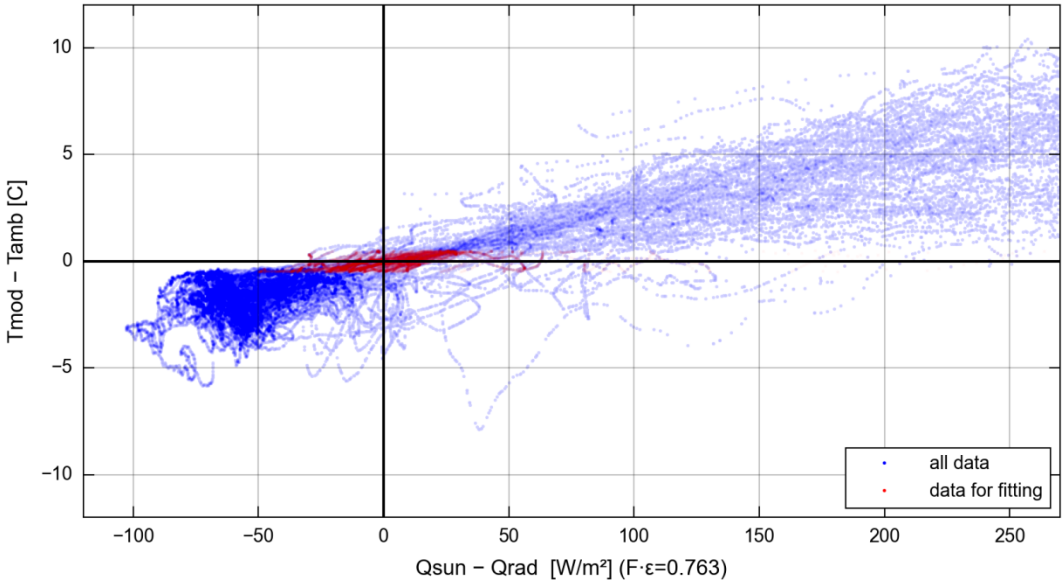


**Figure 6 Close-up of the same data, but on the x-axis the irradiance is reduced by the amount of radiation lost to the sky. The red points representing equilibrium conditions are now centered around the origin as they should be.**

Three cases are evaluated for comparison to the expected values: 35° tilt and horizontal positions in Albuquerque, New Mexico and 25° tilt in Freiburg, Germany. The three $F{\cdot}\varepsilon$ values thus obtained from the field data are plotted in Figure 7 in comparison to the range of expected values, based on the view factors and glass emissivities discussed in section 3.3. All three experimental values lie roughly within the expected range, and the reduction in view factor with increasing tilt angle is observable. Of course three points cannot be considered a complete validation; that could only be achieved by taking new measurements at a variety of tilt angles.

An important secondary observation is that the $F{\cdot}\varepsilon$ product is very sensitive to the temperature difference $T_m - T_a$, and these values were only achieved after incorporating the temperature difference between the back of the module, where the short-wave radiation is absorbed, and the front of the glass, from where the thermal energy is radiated to the sky. Therefore, this fitting technique would likely not work very well with generic data collected from operating PV systems; for optimal performance, this method requires high-quality test-field data. The corollary to this is that the temperature difference is not very sensitive to the value of the $F{\cdot}\varepsilon$ product, and hence low precision and low accuracy may be quite acceptable for module temperature modeling.

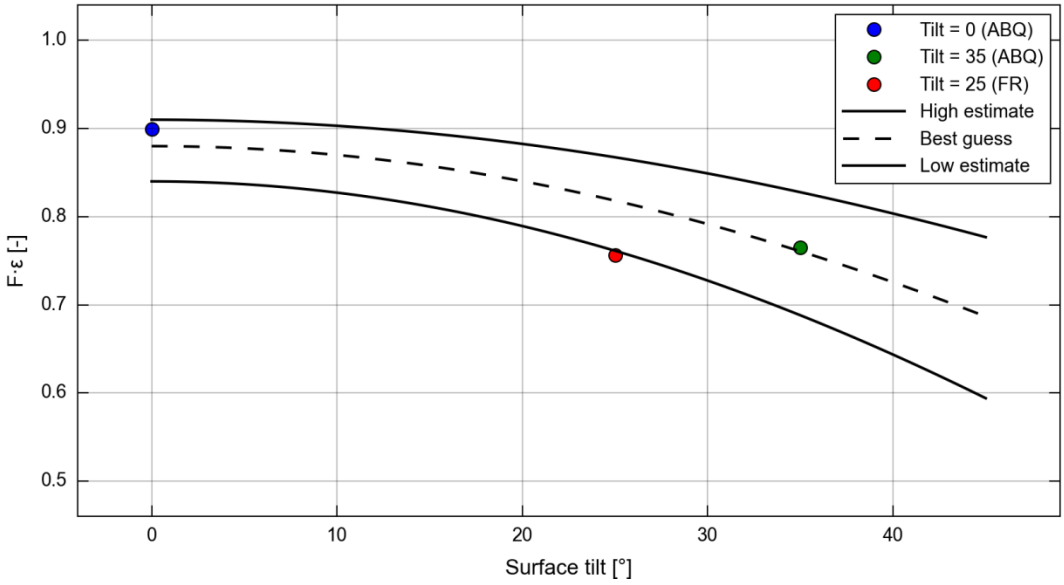


**Figure 7 Three observed values of the product *F·ε* (dots) fall within the expected range (lines) based on different view factor assumptions, as discussed in section 3.3.**

## 5.0 APPLICATION

PV module temperature models are used in simulations to predict module temperature, but prior to this the model parameters values must be determined. Frequently these values are simply obtained from databases, or some default values are used, but all empirical values have their origin in temperature measurements. Numerical fitting procedures are then used to find the model parameters that allow the model to best reproduce the measurements. The definition of "best" can vary substantially: for example, the IEC 61853-2 standard procedure minimizes the RMS error of the implicit heat transfer coefficients using a subset of available data representing stable conditions. A more general approach for fitting model parameters is to minimize the RMS error of the model output—which is PV module temperature in this context.

One of the challenges of fitting a simple model to a more complex phenomenon is that the optimal parameter values may be sensitive to the data selection. A trivial example is fitting a straight line to points lying on a curve: the section of the curve in question and the distribution of the points on that section both influence the slope of such a line. On the other hand, a model that perfectly represents a phenomenon can be fit to any selection of points with the same result (disregarding measurement error). For example, the coefficients of model that is a quadratic equation can be found from any set of three distinct measurement points. Adding the radiative loss term to any of the PV module temperature models discussed in Section 2 brings these models closer to reality, and should therefore both improve temperature predictions and the robustness of parameter fitting.

In this section we briefly present the results of fitting the Faiman model with and without the radiative loss term to one year of measurements. For this purpose we use the estimated value $F{\cdot}\varepsilon = 0.76$, which was also confirmed by observations as reported in Section 4.3. Down-welling radiation is obtained from the ERA5 reanalysis database as discussed in Section 3.2 and interpolated to the one-minute time interval of the module temperature and weather data.

For each model variation the two optimal parameters values are found using a non-linear least-squares method to minimize the RMS-error of the predicted temperature during daytime (solar zenith angle < 90°). The MBE and RMSE are then calculated separately for day and night. Table 2 lists the parameter values as well as the error values). The model errors are also plotted as a function of module temperature in Figure 8, and the distributions of the residuals are shown in Figure 9.

It is evident from both the numeric indicators and the graphical representations that using the proposed radiative loss term leads to substantially better fits on the daytime data: the mean bias error is reduced by nearly 1°C to near zero and the RMSE is reduced by 30%. The improvements in the night-time model predictions are even more substantial, especially considering that no night-time data were used for the parameter determination. Although night-time module temperature is not directly relevant for power generation, this improvement is clear evidence that the modified model is more closely aligned with reality.

**Table 2 Results of fitting the Faiman model with and without the radiative loss term**

| Model variation | $u_0$ | $u_1$ | MBE day [°C] | RMSE day [°C] | MBE night [°C] | RMSE night [°C] |
|---|---|---|---|---|---|---|
| Faiman (standard) | 24.07 | 3.29 | 0.85 | 2.43 | 3.75 | 4.07 |
| Faiman (modified) | 20.74 | 2.91 | −0.03 | 1.68 | 0.84 | 1.53 |

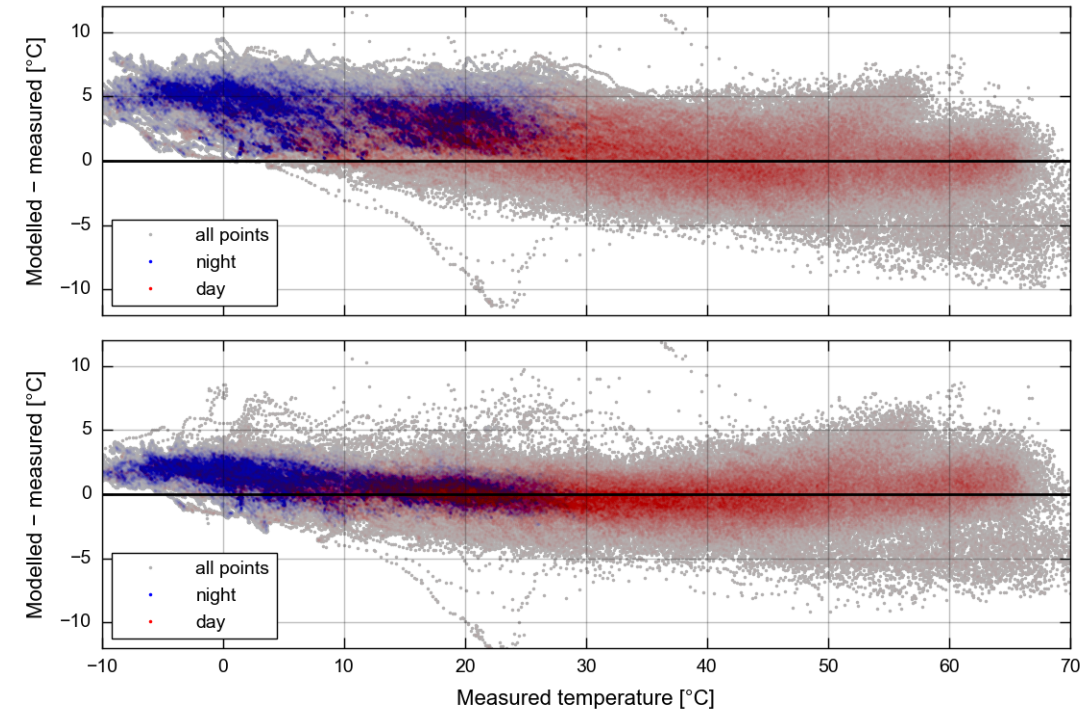


**Figure 8 Model errors using the standard Faiman model (upper) and modified Faiman model (lower). The color saturation of the day and night points indicates point density. The radiative term clearly reduces the skew and scatter.**

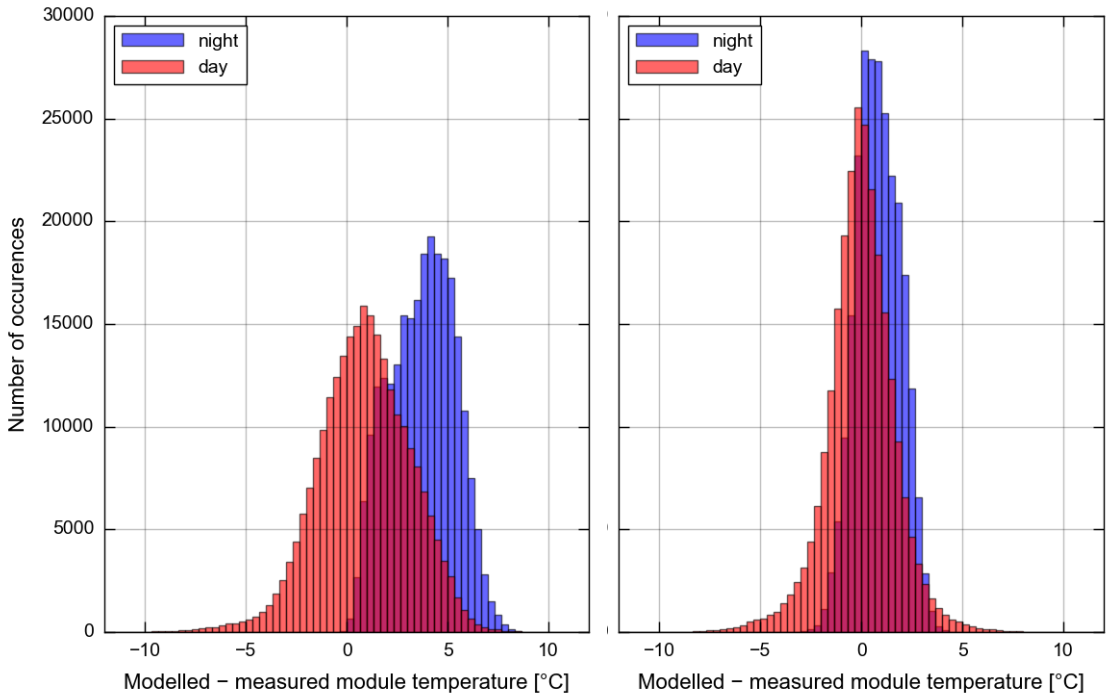


**Figure 9 Model error distributions from the standard Faiman model (left) and modified Faiman model (right). The radiative term reduces the frequency of larger errors (see RMSE in Table 2) and brings both day and night data into better alignment (see MBE in Table 2).**

## 6.0 SUMMARY AND CONCLUSIONS

In this work we have shown how a new radiative loss term can be used to improve any of the four commonly used module operating temperature models without increasing the complexity of module temperature calculations in simulations. The key to retaining simplicity is to separate the total radiative loss into two parts with ambient temperature serving as an intermediate between sky and module temperature. In addition to improving the alignment of the models with observed behavior, the new term introduces new flexibility to adjust for different situations: down-welling long wave radiation, view factor and emissivity are site-specific, installation-specific and module-specific factors respectively.

The new required input data for the improved models, down-welling thermal radiation or equivalent sky temperature, can be readily obtained from global weather models such as the ERA5 reanalysis dataset from ECMWF. Thus, there is no significant barrier to begin incorporating radiative losses into PV system performance simulation software and practices. To support such a transition, candidate data sources should be further evaluated and compared to provide more specific guidance on their use.

The emissivity of PV module front and back surfaces is subject to substantial uncertainty arising from lack of details and context for the range of values reported in the literature. This could in principle be resolved very easily by taking new emissivity measurements on a selection of commonly used materials and publishing them together with all other relevant related information about the materials and methods. Ideally front and back surface long-wave emissivity would be measured during PV modules type approval process and reported on specification sheets in the future.

In this work we have also shown that it is inaccurate to assume an isotropic distribution of down-welling long-wave radiation for the purpose of estimating the needed view factors. Since view factors are installation-specific, further investigation is needed to determine the influence of factors such as tilt angle, and also more complex factors like adjacent PV module rows. Using the techniques described in this report and a variety of purpose-built experimental set-ups, new empirical models for long-wave sky view factor can be developed and validated. Additionally, data collected during the rest of the day can serve to provide much-needed insights into the effect of installation the same variables on convective heat losses.

Finally, we have presented a modest and effective improvement that appears ready for adoption. However, this work has also led to further insights into module temperature modeling, and additional modeling improvements that are under development now.

## REFERENCES


[1] D. Faiman, "Assessing the outdoor operating temperature of photovoltaic modules," *Prog. Photovolt: Res. Appl.*, vol. 16, no. 4, pp. 307–315, Jun. 2008, doi: 10.1002/pip.813.

[2] D. L. King, W. E. Boyson, and J. A. Kratochvil, "Photovoltaic array performance model.," SAND2004-3535, 919131, Aug. 2004. doi: 10.2172/919131.

[3] PVsyst SA, "Project design > Array and system losses > Array Thermal losses," *PVsyst 7 Help*, Jan. 25, 2022. https://www.pvsyst.com/help/thermal_loss.htm (accessed Jan. 25, 2022).

[4] P. Gilman, N. A. DiOrio, J. M. Freeman, S. Janzou, A. Dobos, and D. Ryberg, "SAM Photovoltaic Model Technical Reference Update," NREL/TP--6A20-67399, 1429291, Mar. 2018. doi: 10.2172/1429291.

[5] M. K. Fuentes, "A Simplified Thermal Model for Flat-Plate Photovoltaic Arrays," Sandia National Laboratories, SAND85-0330, May 1987.

[6] NREL, "System Advisor Model (SAM) Release Notes," Dec. 02, 2021. https://nrel.github.io/SAM/doc/releasenotes.html (accessed Apr. 05, 2022).

[7] A. Driesse, Theristis, Marios, and Stein, Joshua S., "PV Module Operating Temperature Model Equivalence and Parameter Translation," presented at the 49th Photovoltaic Specialist Conference (PVSC), Philadelphia, PA, USA, Jun. 2022.

[8] Anton Driesse, "Temperature model parameter translation · Issue #1442 · pvlib/pvlib-python," *GitHub*. https://github.com/pvlib/pvlib-python/issues/1442 (accessed May 30, 2022).

[9] ECMWF, "Climate reanalysis | Copernicus," 2022. https://climate.copernicus.eu/climate-reanalysis (accessed Apr. 26, 2022).

[10] T. J. Silverman *et al.*, "Reducing Operating Temperature in Photovoltaic Modules," *IEEE J. Photovoltaics*, vol. 8, no. 2, pp. 532–540, Mar. 2018, doi: 10.1109/JPHOTOV.2017.2779842.

[11] M. Muller, B. Marion, and J. Rodriguez, "Evaluating the IEC 61215 Ed.3 NMOT procedure against the existing NOCT procedure with PV modules in a side-by-side configuration," in *2012 38th IEEE Photovoltaic Specialists Conference*, Jun. 2012, pp. 000697–000702. doi: 10.1109/PVSC.2012.6317705.

[12] L. Wen, "An Investigation of the Effect of Wind Cooling on Photovoltaic Arrays," Jet Propulsion Laboratory, Mar. 1982.

[13] Dimitri Klebe, "All Sky Infrared Visible Analyzer & All Sky Imaging System Technical Description," Solmirus Corporation, Colorado Springs, Apr. 2021.

[14] A. Driesse, W. Zaaiman, D. S. Riley, N. Taylor, and J. S. Stein, "Indoor and Outdoor Evaluation of Global Irradiance Sensors," in *31st European Photovoltaic Solar Energy Conference and Exhibition; 1704-1709*, 2015, p. 6 pages, 11036 kb. doi: 10.4229/EUPVSEC20152015-5CO.5.3.

[15] P. J. Huber, "Robust Estimation of a Location Parameter," *Ann. Math. Statist.*, vol. 35, no. 1, pp. 73–101, Mar. 1964, doi: 10.1214/aoms/1177703732.

## DISTRIBUTION

**Email—Internal**

| Name | Org. | Sandia Email Address |
|---|---|---|
| Technical Library | 1911 | sanddocs@sandia.gov |

This page left blank

Sandia National Laboratories

Sandia National Laboratories is a multimission laboratory managed and operated by National Technology & Engineering Solutions of Sandia LLC, a wholly owned subsidiary of Honeywell International Inc. for the U.S. Department of Energy's National Nuclear Security Administration under contract DE-NA0003525.